Biosensors and Bioelectronics: X 13 (2023) 100313

Contents lists available at ScienceDirect

Biosensors and Bioelectronics: X

journal homepage: www.journals.elsevier.com/biosensors-and-bioelectronics-x

Detection of serum calprotectin based on molecularly imprinted photonic hydrogels: A novel approach for IBD diagnosis

Sara Resende [a,c], Manuela F. Frasco [b,*], Paulo P. Freitas [c], M. Goreti F. Sales [a,b,**]

[a] BioMark@ISEP/CEB – LABBELS, School of Engineering, Polytechnic Institute of Porto, Porto, Portugal
[b] BioMark@UC/CEB – LABBELS, Department of Chemical Engineering, Faculty of Sciences and Technology, University of Coimbra, Coimbra, Portugal
[c] International Iberian Nanotechnology Laboratory (INL), Braga, Portugal

ARTICLE INFO

Keywords:
Photonic crystals
Molecularly imprinted hydrogels
Serum calprotectin
Inflammatory bowel disease
Biosensors

ABSTRACT

Inflammatory bowel disease (IBD) affects millions of people worldwide, and current diagnosis relies on a number of complex procedures. The need for sensitive diagnostic tools has focused research on discovering new biomarkers and improving detection methods. Serum calprotectin has recently emerged as a new serological biomarker and shows great potential due to its high specificity. In this work, a label-free biosensor combining molecularly imprinted hydrogels and photonic crystals for the detection of serum calprotectin is presented. The unique inverse opal polymer network with imprinted selective binding sites for serum calprotectin enables a highly sensitive, selective, and fast response. The hierarchical structure combined with the molecular recognition process resulted in swelling of the molecularly imprinted photonic hydrogel (MIPH) when binding the target protein. This effect resulted in a readable shift in the reflection peak to longer wavelengths. The analytical performance of the MIPH was demonstrated by a linear response to clinically relevant calprotectin levels and the achievement of a detection limit of 0.07 ng mL^{-1} in serum samples. In addition, the sensor proved to be selective for calprotectin when tested for C-reactive protein, another important biomarker of inflammation. In conclusion, this novel approach was successfully used to determine calprotectin concentrations at clinically relevant levels and provides a rapid and effective alternative for IBD diagnosis and medical analysis.

1. Introduction

Inflammatory bowel diseases (IBDs) are chronic inflammatory disorders of the gastrointestinal tract that affect more than 6.8 million people worldwide, and the incidence is increasing (Alatab et al., 2020). Although IBD is considered an umbrella term, the two main forms are ulcerative colitis (UC) and Crohn's disease (CD). Symptoms include abdominal pain, mucus defection, bowel obstruction, and bleeding (Sairenji et al., 2017). Invasive diagnostic measurements are uncomfortable for patients, but also expensive, and all examinations are considered time-consuming (Azramezani Kopi et al., 2019; Tontini et al., 2015).

Therefore, many studies have been conducted to find suitable biomarkers that could provide the required sensitivity and selectivity for IBD diagnosis. Measurement of C-reactive protein (CRP) is one of the gold standard methods, as this protein is commonly associated with inflammation (Cury et al., 2013; Vermeire et al., 2004). Another common diagnostic method is fecal calprotectin measurement. Calprotectin is a calcium-binding protein of the S100 family (S100A8 and S100A9) that is expressed by leukocytes and is frequently released during infections and inflammatory events (Oosterwijk et al., 2020; Wang et al., 2018). Fecal calprotectin is routinely used in stool analysis of IBD patients (Fukunaga et al., 2018). However, it has been reported that sensitivity and specificity are inconsistent in different assays and that sample collection is difficult (Azramezani Kopi et al., 2019).

Recently, serum calprotectin (SC) has gained more attention as a biomarker for IBD because it can be easily used in routine practice and is better accepted by patients (Kalla et al., 2016; Meuwis et al., 2013). Several reports have claimed that high levels of SC are correlated with intestinal inflammation in CD (Meuwis et al., 2013) and UC (Malham

* Corresponding author. BioMark@UC/CEB – LABBELS, Department of Chemical Engineering, Faculty of Sciences and Technology, University of Coimbra, Coimbra, Portugal.
** Corresponding author. BioMark@UC/CEB – LABBELS, Department of Chemical Engineering, Faculty of Sciences and Technology, University of Coimbra, Coimbra, Portugal.
E-mail addresses: mffrasco@gmail.com (M.F. Frasco), goreti.sales@eq.uc.pt, goreti.sales@gmail.com (M.G.F. Sales).

https://doi.org/10.1016/j.biosx.2023.100313
Received 22 November 2022; Received in revised form 18 January 2023; Accepted 1 February 2023
Available online 10 February 2023

et al., 2019) and thus could be a potential predictor for the diagnosis of IBD (Azramezani Kopi et al., 2019; Cury et al., 2013; Fukunaga et al., 2018; Kalla et al., 2016). Altered SC levels have also been associated with the diagnosis of cancer (Topuz et al., 2017), neonatal sepsis (Decembrino et al., 2015), skin diseases (Tampa et al., 2018), cystic fibrosis (Reid et al., 2015), and rheumatoid arthritis (Hurnakova et al., 2018). The combination of SC with other blood-based biomarkers may help in the treatment of IBD as well as in predicting its long-term outcome (Kalla et al., 2016; McCann et al., 2017).

Currently, levels of SC are measured using commercial ELISA kits, which are expensive, labor intensive, and complex. Therefore, intensive research is being conducted to develop reliable, rapid, and sensitive biosensors for IBD diagnosis (Barra et al., 2020). In addition, the establishment of new biomarkers and biosensors is urgently needed to diagnose and distinguish CD from UC and to track disease activity.

In the field of biosensors, molecularly imprinted polymers (MIPs) have been extensively used as efficient and cost-effective recognition elements that bind to target analytes with high affinity and selectivity (Chiappini et al., 2020; Frasco et al., 2017). These biomimetic elements are used in sensors along with various types of transducers (e.g., electrochemical, optical) to convert recognition events into readable signals (Chen et al., 2016). The combination of molecular imprinting with colloidal-crystal templating is an ingenious field because it creates a transducer platform within the recognition sites and enables the development of label-free biosensors (Inan et al., 2017; Resende et al., 2020).

Many interesting examples of molecularly imprinted photonic hydrogels (MIPHs) have been investigated as novel self-reporting sensor platforms for efficient detection of analytes (Umar et al., 2019). Recent studies report their use for environmental (Huang et al., 2018; Wang et al., 2013), forensic (Meng et al., 2013), and medical purposes (Tang and Chen, 2020; Wu et al., 2008). This type of sensor combines the structural color of self-assembled colloidal particles with imprinted polymers. If the colloidal particles are removed, the result is a highly ordered three-dimensional macroporous structure that can optically respond to chemical stimuli, enabling analyte detection. In such hierarchical structure, the molecular recognition process induces swelling or shrinking of the MIPHs, and the optical response enables analyte detection (Chen et al., 2017). Analyte binding alters the periodic lattice spacing and refractive index, resulting in a shift in Bragg diffraction and a visually perceptible color change (Armstrong and O'Dwyer, 2015; Vaz et al., 2020).

To the best of our knowledge, the present work is the first to develop a label-free colorimetric detection of SC. The proposed approach relies on the high sensitivity and selectivity of MIPHs to provide a rapid and cost-effective sensor technology that can be readily implemented in point-of-care assays for the management of IBD patients in the future. This new sensor design and construction process is illustrated in Fig. 1. A highly ordered 3D scaffold is obtained by self-assembly of poly (methyl methacrylate) (PMMA) spheres. The interstices within the opal structure were filled with the pre-polymerization solution containing the target protein SC. After photopolymerization, simultaneous degradation of the sacrificial spheres and removal of the template allowed the generation of an inverse opal hydrogel structure containing the specific recognition cavities for SC. During detection, there is a gradual red shift in the reflection wavelength of the MIPH. The sensor for SC showed not only a fast response but also good selectivity for the target molecule, which is very promising for future applications in IBD diagnosis.

2. Experimental

2.1. Reagents

Serum calprotectin (SC), S100A8/A9, was obtained from BioLegend; C-reactive protein (CRP) from human fluids, methyl methacrylate, acrylamide (AAm), N,N'-methylenebis (acrylamide) (Bis-AAm), 2,2-dimethoxy-2-phenylacetophenone, methanol and sulfuric acid were obtained from Sigma-Aldrich; Phosphate Buffered Saline (PBS) tablets were from Amresco; Acetone and hydrogen peroxide were acquired from LabChem. All solutions were prepared with ultra-pure water (conductivity <0.1 μS cm^{-1}). All reagents were of analytical grade and were used as acquired without further purification. Glass slides were obtained from Deltalab and cut into small pieces (1 cm length) before use. Piranha solution was used for hydrophilic treatment of glass slides.

2.2. Synthesis of PMMA colloidal spheres

Monodisperse PMMA spheres were prepared via surfactant-free emulsion polymerization (Pereira et al., 2022). Briefly, potassium persulfate (1.83×10^{-3} mol L^{-1}) was added to an aqueous solution of methyl methacrylate monomer (1.09 mol L^{-1}) under inert atmosphere at reflux and constant agitation (300 rpm). The polymerization reaction occurred at 100 °C and was stopped after 2 h. The obtained particle suspension was washed with ultra-pure water by several rounds of centrifugation (8000 rpm for 15 min).

2.3. Preparation of the inverse opal hydrogel

First, the opal photonic crystals were prepared via vertical deposition

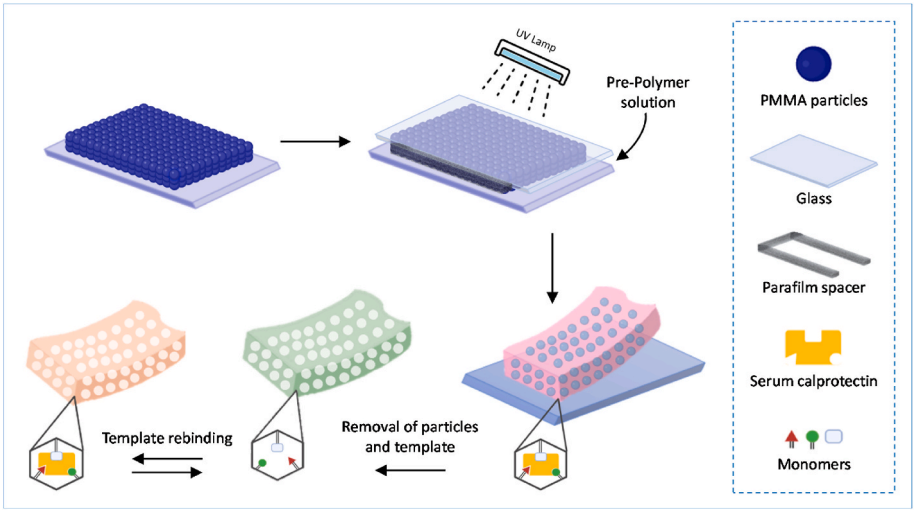

Fig. 1. Schematic representation of MIPH sensor construction for detection of serum calprotectin.

of PMMA colloidal particles in clean glass substrates. This process was performed in an oven for 2 days at 60 °C. Then, the template protein (20 μg mL^{-1}) was pre-incubated with the functional monomer AAm (1.3 mol L^{-1}) in 0.010 mol L^{-1} PBS for 2 h at 4 °C. Next, the cross-linker Bis-AAm (0.03 mol L^{-1}) and the initiator 2,2-dimethoxy-2-phenylacetophenone (0.008 mol L^{-1}) were added to the solution, followed by nitrogen purging. The glass of PMMA photonic crystal was covered with glass slides on both sides, with Parafilm® spacers, and tightly held together. The polymerization solution was introduced with a syringe into the space between the glass slides. Once the colloidal crystal template became transparent, all gaps between the spheres were filled. Photopolymerization was carried out under 365 nm light for 3 h and the polymerized hydrogel was then immersed in ultra-pure water to separate the glass slides. Next, the obtained MIPH was immersed in a mixture of acetone and water to remove the PMMA spheres and the template protein. A non-imprinted photonic hydrogel (NIPH) was prepared as control material by the same method without addition of the template molecule.

2.4. Characterization of materials and optical measurements

The size of PMMA spheres was measured using transmission electron microscopy (TEM). The sample (10 μL) was mounted on Formvar/carbon film-coated mesh nickel grids (Electron Microscopy Sciences, Hatfield, PA, USA) and left standing for 2 min. Visualization was carried out on a JEOL JEM 1400 TEM at 120 kV (Tokyo, Japan). Images were digitally recorded using a CCD digital camera Orious 1100 W Tokyo, Japan.

The hydrodynamic diameter, polydispersity index, and zeta potential of PMMA spheres were analyzed by dynamic light scattering (DLS) using a Malvern Zetasizer Nano ZS (Malvern Instruments Ltd., UK).

The assembled PMMA photonic structure on glass and the morphology of the photonic hydrogel samples were investigated by Scanning Electron Microscopy (SEM) on a FEI Quanta 400 FEG ESEM. Prior to analysis, samples were coated with a thin film of Au/Pd using the SPI Module equipment.

For optical measurements, a reflection fibre probe (fibre diameter of 200 μm, Dropsens), and a deuterium-halogen light source along with a spectrophotometer (wavelength range of 200–1100 nm, Methrom, AG) were used. A diffuse reflectance standard was used as a reference surface and the reflectance at 45° incidence was collected using the optical fibre probe.

2.5. Detection of SC with MIPH film

The sensing properties of the MIPH film were first evaluated in PBS buffer, with SC solutions ranging from 0.1 to 7812.5 ng mL^{-1}. All solutions were freshly prepared, and all experiments were carried out at room temperature. Initially, MIPH sensor was stabilized in PBS buffer, followed by successive incubations with SC for 40 min before reflection spectra were collected. For the calibration studies in human serum, Cormay serum HN (PZ Cormay S.A.) was used with 1000-fold dilution in PBS buffer to a final SC concentration range of 0.1–9.8 ng mL^{-1}.

Sensor responses were analyzed by relative wavelength shift $(\lambda-\lambda_0)/\lambda_0$, where λ_0 is the wavelength of the maximum intensity of the blank and λ corresponds to the wavelength of the maximum intensity for each protein standard. Calibration plots of optical signal against the logarithm concentration of SC were evaluated with regard to the linear regression obtained. The limit of detection (LOD) was calculated as the concentration taken at the point of intersection of the fitted linear curve (at the minimum 95% confidence limit) and a line parallel to the x-axis through the mean intensity value measured in the lowest concentration (Buck and Lindner, 1994).

Additionally, practical applicability was confirmed by testing the MIPH sensor with SC and CRP, one of the most common biomarkers correlated with inflammation and infection processes (Ishida et al., 2021; Vermeire et al., 2004). Studies were performed in serum, also 1000-fold diluted, with SC final concentrations of 1.0 and 8.5 ng mL^{-1} and CRP of 10.0 and 400.0 ng mL^{-1}, separately and combined. Each solution was incubated for 40 min, the same period used in the calibration procedure.

In all experiments, at least three independent replicates using independent sensors were performed, and results are presented as average with standard deviation (SD). All conditions were also tested on NIPH as control.

3. Results and discussion

3.1. Characterization of PMMA colloidal spheres and hydrogel film

The microscopy analyses confirmed the successful synthesis of PMMA colloidal spheres with a diameter of around 200 nm (Fig. 2A). The colloidal suspension was also analyzed by DLS, and the measurements gave an average hydrodynamic diameter of 247.4 ± 1.5 nm. This difference in the size was expected because the hydrodynamic size given by DLS includes an electrical double layer around the particle. Moreover, the apparent hydrodynamic size is larger in the current measurements at low concentration ionic medium (Schumacher and van de Ven, 1987). From DLS measurements, a polydispersity index of 0.039 ± 0.030 was obtained. As this dimensionless parameter determined by the cumulants analysis was below 0.7, it suggests that the suspension had a narrow particle size distribution (Danaei et al., 2018). The zeta potential measurements showed that the particles had a negative surface charge of about −59.4 ± 0.6 mV, indicating that the dispersion is stable due to electrostatic repulsion between the particles. The monodisperse, spherical colloids of PMMA enabled to obtain a self-assembled photonic crystal with a close-packed structure, as depicted by the SEM image (Fig. 2B) and presenting a smooth brilliant color (Fig. 2C). This highly ordered array is one of the requisites for MIPH preparation.

The infiltration of the pre-polymer mixture is the other key aspect to accomplish the diffusion of the solution in the interstitial space between the spheres and a homogenous polymer. After polymerization, the SEM analysis showed that the opal structure was preserved in the MIPH (Fig. 3A). After removal of PMMA sacrificial particles and the template, a negative imprinting remained (Fig. 3B). After polymer infiltration, in comparison to the opal film on glass, there was a red shift in the reflectance peak as the hydrogel leads to an increase in the lattice spacing (Fig. 3E). The interstitial filling of the PMMA spheres organized on glass with the hydrogel also originates a decrease in the refractive index contrast, accompanied by positive change in the average refractive index, and leading to a red shift of the peak (Goerlitzer et al., 2018; Phillips et al., 2016). After removal of the PMMA spheres and the template protein, a blue shift is observed (Fig. 3E), consistent with a decrease in the periodicity due to hydrogel shrinkage, resulting from converting the close-packed photonic crystal into air spheres, and contraction of the macropores, as well as of the imprinted cavities in the case of MIPH. (Feng et al., 2019; Griffete et al., 2011; Liu et al., 2012). A similar behavior was observed in the NIPH, with the incorporation of the opal film in the hydrogel (Fig. 3C) and obtaining an inverse opal (Fig. 3D), also observed in the reflectance spectra (Fig. 3E). As reported in the literature, structured polymer hydrogels can swell and shrink leading to a shift of Bragg diffraction peak. In crosslinked networks, the swelling behavior is a function of the crosslinking density and chemistry (Griffete et al., 2012; Martens and Anseth, 2000). The differences observed between the NIPH and MIPH shifts in the reflectance peaks when PMMA particles and the template protein are removed can be explained mainly due to variations in the network structure of the hydrogel (Griffete et al., 2012; Martens and Anseth, 2000). The protein incorporation during polymerization may result in a lower crosslinking density and a more porous network in MIPH since the polymer will form around the template protein, which will leave additional empty nanocavities in comparison to NIPH. These differences may account for the

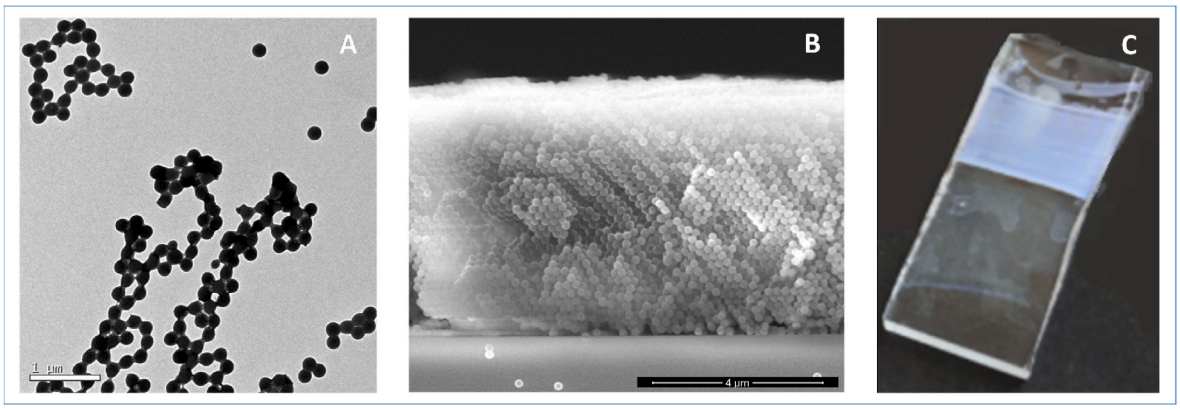

Fig. 2. Analysis of PMMA colloidal particles by TEM (A) and after self-assembly on glass, as imaged by SEM (B) and a photograph of the colored photonic structure (C).

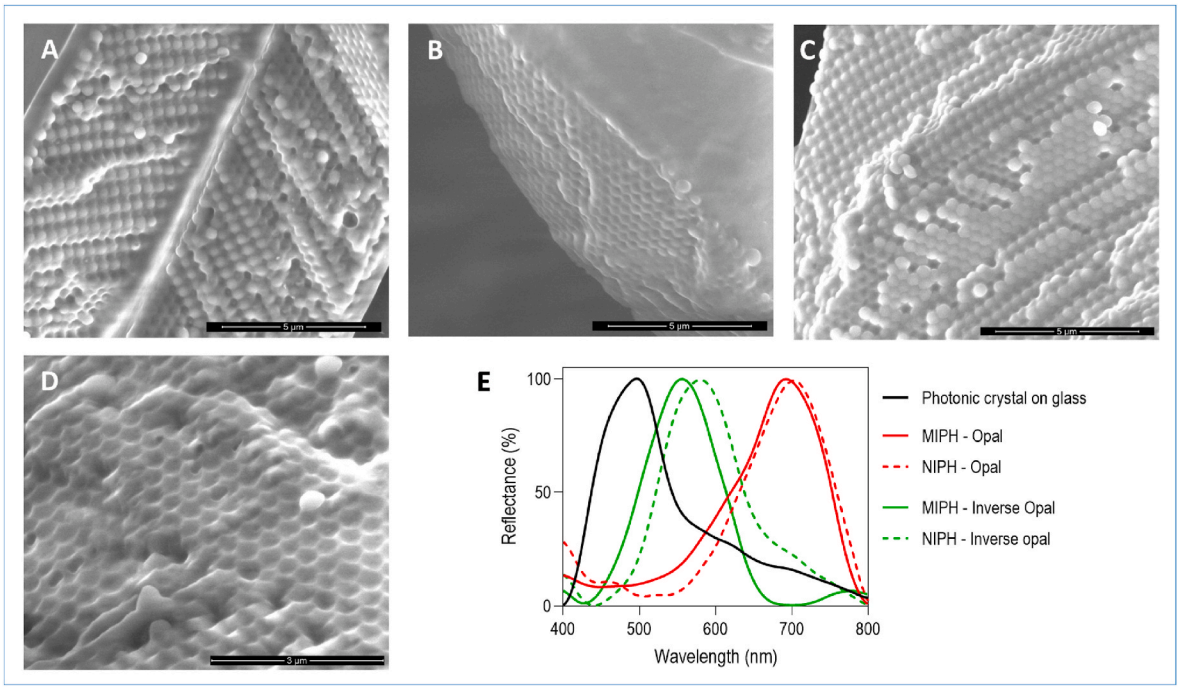

Fig. 3. Biosensor construction followed by SEM analysis: MIPH – Opal (A), MIPH – Inverse Opal (B), NIPH – Opal (C), NIPH – Inverse Opal (D); and reflectance spectroscopy, showing representative normalized spectra of the optical materials (E).

different change of the periodic lattice spacing when obtaining the inverse opal hydrogels, as MIPH shifted to smaller wavelengths, but also may be relevant for the recognition ability of MIPH (Griffete et al., 2012).

3.2. Sensing properties of MIPH to SC

Both MIPH and NIPH were incubated with increasing concentrations of SC to trace calibration curves for the sensing material. Different conditions were tested to this end by analyzing sensor response in PBS buffer and serum, with respective blank controls. Upon incubation with increasing concentrations of SC in PBS buffer, the reflection wavelength of the MIPH was shifted to longer wavelengths (Fig. 4A), while the NIPH had random variation (Fig. 4B). As expected, and following the Bragg-Snell's law, the red shift can be explained by the ability of the hydrogel network to recognize and bind the specific SC target and swell, as reported in previous studies (Griffete et al., 2012; Jinn et al., 2019; Li et al., 2011). The random variation of the reflectance peak in NIPH corroborates the necessity of selective imprinted binding sites for recognition and biosensor response. In terms of analytical features of the MIPH calibration in buffer, a linear relationship was displayed between the relative shift of the diffraction peak and the logarithm SC concentration ranging from 0.1 to 7812.5 ng mL^{-1} (Fig. 4C). The LOD was found to be 0.06 ng mL^{-1}.

Considering that the main aim of this work is to provide a novel tool to measure the levels of calprotectin in serum, studies proceeded by testing MIPH, and the respective NIPH control, in serum, a highly complex matrix. To this end, calibration studies were performed with standard solutions prepared in serum 1000-fold diluted in PBS buffer. The tested concentrations of SC ranged from 0.10 to 9.77 ng mL^{-1}, considering that in real sample analyses those concentrations are 1000-fold higher. The obtained results showed a red shift of about 11 nm upon protein incubation, and a linear response in the range of tested concentrations (Fig. 4D). By contrast, no shift was observed in the NIPH, indicating that a non-specific interaction with SC causes the random variation in the sensor response (Fig. 4E). In serum, a LOD of 0.07 ng

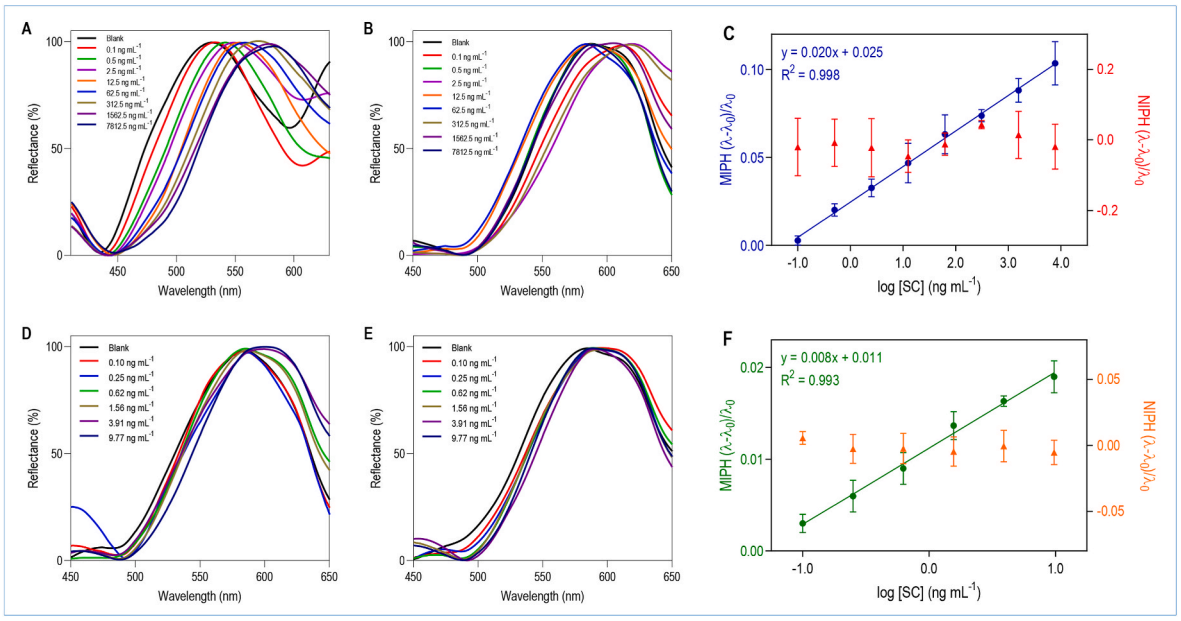

Fig. 4. Analytical response to increasing concentrations of SC: representative normalized reflectance spectra of MIPH (A, D), respective NIPH controls (B, E) and corresponding calibration curves (C, F) in buffer (A–C) and serum (D–F) (mean ± SD of minimum n = 3).

mL^{-1} was obtained, which is higher, but not significantly, than the LOD determined in PBS buffer. Moreover, the slope of the calibration curve in PBS is also higher, suggesting that the sensitivity in serum was reduced. Nonetheless, the sensor still responded to low levels and short range of SC concentrations in a complex matrix, namely at concentrations of clinical interest, which is very promising considering future applications (Fig. 4F). In addition, the standard deviation of the calibration points in the linear trend ranged from 0.1% (minimum) to 1.2% (maximum) in both buffer and serum calibrations, confirming the repeatability of the sensor response.

Various clinical studies have reported that the levels of SC in diseased subjects can rise to almost 8800 ng mL^{-1}, while values in healthy patients are around 1300 ng mL^{-1} (Kalla et al., 2016; Leach et al., 2007; Meuwis et al., 2013). This label-free sensor is able to detect SC in the presence of a complex mixture of compounds in the serum, in the range of clinical interest. Thus, the proposed biosensor can be considered a valuable tool in providing quick and low-cost information concerning the levels of SC in both healthy and diseased conditions.

There are only a few reports in the literature for SC detection, being most of these methods based on ELISA assays. The ELISA methods, although sensitive and presenting high accuracy and robustness, are associated with high-costs and time-consuming procedures (Fukunaga et al., 2018; Martinez Valenzuela et al., 2018; Nilsen et al., 2015; Rogler et al., 2013). Despite this biomarker being correlated with other conditions, innovative methods for calprotectin detection are still in high demand (Hauzer et al., 2021). Few examples can be found in the literature regarding biosensors for calprotectin detection. An enzyme-free electrochemical immunosensor based on functionalized metal-organic framework has been proposed and the amperometric current response enabled ultrasensitive detection of calprotectin with linear range from 200 fg mL^{-1} to 50 ng mL^{-1} and LOD of 137.7 fg mL^{-1} (Dong et al., 2020). Recently, a DNAzyme-based assay was developed and the turn-off fluorescence in the presence of calprotectin originated a LOD of 9.89 nmol L^{-1} with 10–200 nmol L^{-1} linear range (Si et al., 2022). Thus, the results obtained with the current photonic hydrogel are very good in comparison to previously reported techniques, appearing as a simple and affordable method with LOD at clinically relevant values. These works may promote further development of low-cost biosensors with quick responses that would not only allow the test results to be available on-site, but it would also reduce the costs for healthcare centers and laboratories.

3.3. Sensing accuracy and MIPH selectivity

In order to evaluate the accuracy of the sensor, optical readings were performed in serum 1000-fold diluted that was spiked with two different concentrations of SC, 1.0 ng mL^{-1} and 8.5 ng mL^{-1}, representing healthy and diseased individuals, respectively, and considering serum dilution factor (Kalla et al., 2016; Vermeire et al., 2004). MIPH results were consistent with the spiked levels (Fig. 5A). The lowest value of 1.0 ng mL^{-1} shifted within 4% of the theoretical concentration with a relative standard deviation (RSD) of 17% (n = 3). For the highest value of 8.5 ng mL^{-1}, the bias was 3% and the RSD was 26% (n = 3). These results suggest that the sensing material developed enables an accurate analysis of the SC biomarker within the tested concentration range.

The selectivity of the sensor was evaluated by investigating the recognition ability of CRP, another relevant biomarker strongly associated with inflammation (Chang et al., 2015). The concentrations used for this purpose were 1.0 ng mL^{-1} and 8.5 ng mL^{-1} for SC and 10.0 ng mL^{-1} and 400.0 ng mL^{-1} for CRP, all prepared in 1000-fold diluted serum. As previously indicated, these concentrations were chosen according to the estimated values in healthy and diseased individuals, respectively, after correcting for serum dilution factor. Selectivity studies were performed first by evaluating sensor response to CRP. Then, the presence of CRP in a mixture with SC was assessed to determine if CRP would interfere with sensor response. When incubated with CRP at 10.0 ng mL^{-1} and 400.0 ng mL^{-1}, MIPH had a negligible response (Fig. 5B). These results suggest that the MIPH is not able to recognize CRP, which is further corroborated by the significative response of MIPH to SC in much lower concentrations than CRP. Moreover, when testing solutions containing both SC and CRP, the results evidenced that CRP did not interfere with SC detection because the observed peak shifts regarding the blank are similar to the shifts observed when testing SC alone (Fig. 5B). The obtained data provides evidence of the selectivity of the MIPH towards SC, which elucidates that molecular imprinting plays a key role in the recognition. This indicates the cooperative effect of the shape, size, and interaction chemistry of the formed binding sites, with all of them playing a critical role in the high selective recognition process (Saylan et al., 2019).

These results evidenced the very good selectivity features of the

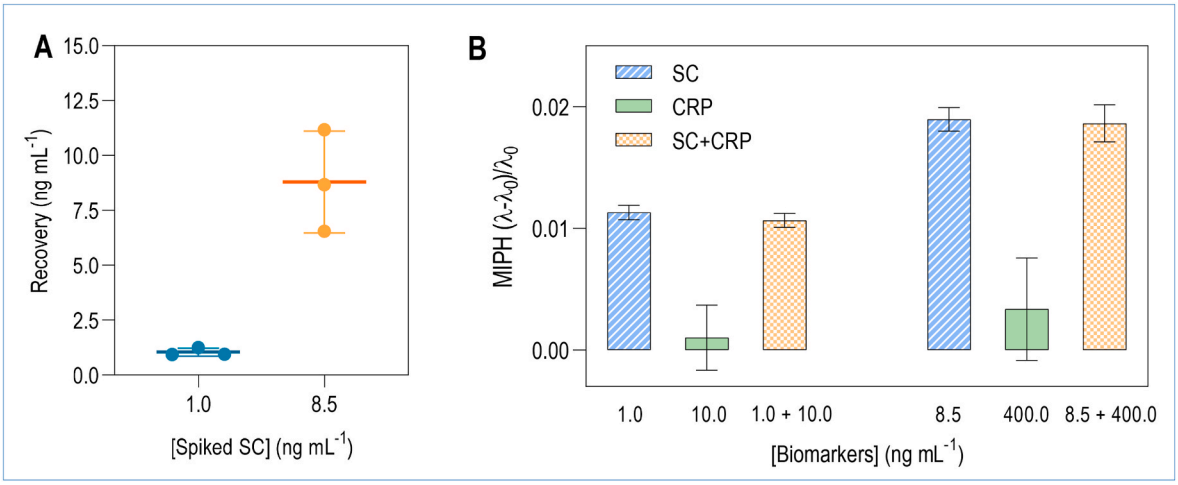

Fig. 5. (A) Recovery assays using MIPH sensor after spiking serum with 1.0 and 8.5 ng mL^{-1} of SC; (B) Selective response of MIPH when incubated with SC (1.0 and 8.5 ng mL^{-1}), with CRP (10.0 and 400.0 ng mL^{-1}), and with a combination of both IBD biomarkers at the lowest (1.0 ng mL^{-1} SC + 10.0 ng mL^{-1} CRP) and highest (8.5 ng mL^{-1} SC + 400.0 ng mL^{-1} CRP) concentrations (mean ± SD of n = 3).

MIPH, confirming a high affinity to the target molecule, rather than a competing biomarker, which originated a selective binding on the imprinted sites and a change in the hydrogel properties inducing a wavelength shift. Together with a sensitive and accurate response, the results are very promising concerning the practical performance of MIPH in real biological samples.

4. Conclusions

In this work, we presented a label-free and sensitive biosensor for detection of SC by combining photonic crystals and molecularly imprinted hydrogels. A simple and inexpensive method enabled to construct a photonic structure by self-assembly of colloidal PMMA, which was then transferred to a selective MIPH after imprinting. Benefiting from the highly ordered structure of the photonic template and the specificity of molecular imprinting technology, MIPH can directly transfer the molecular recognition process into a readable signal. As the imprinted binding sites became increasingly occupied by the target, the internal pore structure of the inverse opal polymeric network was altered, producing an optical response, namely a shift in the reflectance peak. The imprinted-based sensor showed good linearity range and low LOD both in buffer and in serum. Also, the sensing material demonstrated to be selective to SC when tested against CRP, a competing biomarker in these diseases. For real sample applications, the developed system has shown satisfactory accuracy and good reproducibility. In summary, the sensor displayed high sensitivity and selectivity as well as quick response. After further optimization, such biosensor can hopefully be applicable at the point-of-care for improved clinical outcomes in IBD.

CRediT authorship contribution statement

Sara Resende: Investigation, Methodology, Validation, Formal analysis, Data curation, Visualization, Writing – original draft. **Manuela F. Frasco:** Conceptualization, Methodology, Supervision, Writing – review & editing. **Paulo P. Freitas:** Supervision, Writing – review & editing. **M. Goreti F. Sales:** Supervision, Funding acquisition, Writing – review & editing.

Declaration of competing interest

The authors declare that they have no known competing financial interests or personal relationships that could have appeared to influence the work reported in this paper.

Data availability

Data will be made available on request.

Acknowledgments

The authors gratefully acknowledge funding from the European Commission through the project MindGAP (FET-Open/H2020/GA829040). The author Sara Resende acknowledges Fundação para a Ciência e a Tecnologia (FCT) for the PhD grant (SFRH/BD/139634/2018).

References

Alatab, S., Sepanlou, S.G., Ikuta, K., Vahedi, H., Bisignano, C., Safiri, S., 2020. Lancet Gastroenterol 5, 17–30.
Armstrong, E., O'Dwyer, C., 2015. J. Mater. Chem. C 3, 6109–6143.
Azramezani Kopi, T., Shahrokh, S., Mirzaei, S., Asadzadeh Aghdaei, H., Amini Kadijani, A., 2019. Gastroenterol Hepatol Bed Bench 12, 183–189.
Barra, M., Danino, T., Garrido, D., 2020. Front. Bioeng. Biotechnol. 8, 265.
Buck, R.P., Lindner, E., 1994. Pure Appl. Chem. 66, 2527–2536.
Chang, S., Malter, L., Hudesman, D., 2015. World J. Gastroenterol. 21, 11246–11259.
Chen, H., Lou, R., Chen, Y., Chen, L., Lu, J., Dong, Q., 2017. Drug Deliv. 24, 775–780.
Chen, W., Meng, Z., Xue, M., Shea, K.J., 2016. Mol. Impr., 4, pp. 1–12.
Chiappini, A., Pasquardini, L., Bossi, A.M., 2020. Sensors, 20, p. 5069.
Cury, D.B., Mizsputen, S.J., Versolato, C., Miiji, L.O., Pereira, E., Delboni, M.A., Schor, N., Moss, A.C., 2013. Cell. Immunol. 282, 66–70.
Danaei, M., Dehghankhold, M., Ataei, S., Hasanzadeh Davarani, F., Javanmard, R., Dokhani, A., Khorasani, S., Mozafari, M.R., 2018. Pharmaceutics, 10, p. 57.
Decembrino, L., De Amici, M., Pozzi, M., De Silvestri, A., Stronati, M., 2015. J Immunol Res 2015, 147973.
Dong, L., Yin, L., Tian, G., Wang, Y., Pei, H., Wu, Q., Cheng, W., Ding, S., Xia, Q., 2020. Sensor. Actuator. B Chem. 308, 127687.
Feng, X., Xu, J., Liu, Y., Zhao, W., 2019. J. Mater. Chem. B 7, 3576–3581.
Frasco, M.F., Truta, L.A., Sales, M.G., Moreira, F.T., 2017. Sensors, 17, p. 523.
Fukunaga, S., Kuwaki, K., Mitsuyama, K., Takedatsu, H., Yoshioka, S., Yamasaki, H., Yamauchi, R., Mori, A., Kakuma, T., Tsuruta, O., Torimura, T., 2018. Int. J. Mol. Med. 41, 107–118.
Goerlitzer, E.S.A., Klupp Taylor, R.N., Vogel, N., 2018. Adv. Mater. 30, 1706654.
Griffete, N., Frederich, H., Maître, A., Ravaine, S., Chehimi, M.M., Mangeney, C., 2012. Langmuir 28, 1005–1012.
Griffete, N., Frederich, H., Maître, A., Schwob, C., Ravaine, S., Carbonnier, B., Chehimi, M.M., Mangeney, C., 2011. J. Colloid Interface Sci. 364, 18–23.
Hauzer, W., Ferenc, S., Rosinczuk, J., Gnus, J., 2021. Curr. Pharmaceut. Biotechnol. 22, 508–513.
Huang, C., Cheng, Y., Gao, Z., Zhang, H., Wei, J., 2018. Sensor. Actuator. B Chem. 273, 1705–1712.
Hurnakova, J., Hulejova, H., Zavada, J., Komarc, M., Cerezo, L.A., Mann, H., Vencovsky, J., Pavelka, K., Senolt, L., 2018. Clin. Rheumatol. 37, 2055–2062.
Inan, H., Poyraz, M., Inci, F., Lifson, M.A., Baday, M., Cunningham, B.T., Demirci, U., 2017. Chem. Soc. Rev. 46, 366–388.
Ishida, N., Higuchi, T., Miyazu, T., Tamura, S., Tani, S., Yamade, M., Iwaizumi, M., Hamaya, Y., Osawa, S., Furuta, T., Sugimoto, K., 2021. Sci. Rep. 11, 12431.

Jinn, W.S., Shin, M.-K., Kang, B., Oh, S., Moon, C.-E., Mun, B., Ji, Y.W., Lee, H.K., Haam, S., 2019. J. Mater. Chem. B 7, 7120–7128.
Kalla, R., Kennedy, N.A., Ventham, N.T., Boyapati, R.K., Adams, A.T., Nimmo, E.R., Visconti, M.R., Drummond, H., Ho, G.T., Pattenden, R.J., Wilson, D.C., Satsangi, J., 2016. Am. J. Gastroenterol. 111, 1796–1805.
Leach, S.T., Yang, Z., Messina, I., Song, C., Geczy, C.L., Cunningham, A.M., Day, A.S., 2007. Scand. J. Gastroenterol. 42, 1321–1331.
Li, J., Zhang, Z., Xu, S., Chen, L., Zhou, N., Xiong, H., Peng, H., 2011. J. Mater. Chem. 21, 19267–19274.
Liu, F., Huang, S., Xue, F., Wang, Y., Meng, Z., Xue, M., 2012. Biosens. Bioelectron. 32, 273–277.
Malham, M., Carlsen, K., Riis, L., Paerregaard, A., Vind, I., Fenger, M., Wewer, V., 2019. Scand. J. Gastroenterol. 54, 1214–1219.
Martens, P., Anseth, K.S., 2000. Polymer 41, 7715–7722.
Martinez Valenzuela, L., Draibe, J., Quero Ramos, M., Fulladosa Oliveras, X., Melilli, E., Cruzado Garrit, J.M., Torras Ambrós, J., 2018. PLoS One 13, e0205982.
McCann, R.K., Smith, K., Gaya, D.R., 2017. Clin. Biochem. 50, 533–536.
Meng, L., Meng, P.J., Tang, B.G., Zhang, Q.Q., Wang, Y.J., 2013. Forensic Sci. Int. 231, 6–12.
Meuwis, M.A., Vernier-Massouille, G., Grimaud, J.C., Bouhnik, Y., Laharie, D., Piver, E., Seidel, L., Colombel, J.F., Louis, E., 2013. Journal of Crohn's and Colitis 7, e678–e683.
Nilsen, T., Sunde, K., Larsson, A., 2015. J. Inflamm. 12, 45-45.
Oosterwijk, M.M., Bakker, S.J.L., Nilsen, T., Navis, G., Laverman, G.D., 2020. Int. J. Mol. Sci. 21, 8075.
Pereira, C.F., Sales, M.G.F., Frasco, M.F., 2022. Talanta 243, 123387.
Phillips, K.R., England, G.T., Sunny, S., Shirman, E., Shirman, T., Vogel, N., Aizenberg, J., 2016. Chem. Soc. Rev. 45, 281–322.
Reid, P.A., McAllister, D.A., Boyd, A.C., Innes, J.A., Porteous, D., Greening, A.P., Gray, R. D., 2015. Am. J. Respir. Crit. Care Med. 191, 233–236.
Resende, S., Frasco, M.F., Sales, M.G.F., 2020. Sensor. Actuator. B Chem. 312, 127947.
Rogler, G., Aldeguer, X., Kruis, W., Lasson, A., Mittmann, U., Nally, K., Peyrin-Biroulet, L., Schoepfer, A., Vatn, M., Vavricka, S., Logan, R., 2013. Journal of Crohn's and Colitis 7, 670–677.
Sairenji, T., Collins, K.L., Evans, D.V., 2017. PrimaryCare 44, 673–692.
Saylan, Y., Akgönüllü, S., Yavuz, H., Ünal, S., Denizli, A., 2019. Sensors 19, 1279.
Schumacher, G.A., van de Ven, T.G.M., 1987. Faraday Discuss. Chem. Soc. 83, 75–85.
Si, J., Zhou, W., Zhou, D., Fang, Y., Shen, X., Zhu, C., 2022. Chemosensors 10, 495.
Tampa, M., Sarbu, M.-I., Mitran, M.-I., Mitran, C.-I., Matei, C., Georgescu, S.-R., 2018. Dis Markers 2018, 5823684-5823684.
Tang, W.W., Chen, C., 2020. Polymers 12, 625.
Tontini, G.E., Vecchi, M., Pastorelli, L., Neurath, M.F., Neumann, H., 2015. World J. Gastroenterol. 21, 21–46.
Topuz, M.F., Binnetoglu, A., Yumusakhuylu, A.C., Sari, M., Baglam, T., Gerin, F., 2017. Eur. Arch. Oto-Rhino-Laryngol. 274, 2499–2504.
Umar, M., Min, K., Kim, S., 2019. Apl Photonics, 4, 120901.
Vaz, R., Frasco, M.F., Sales, M.G.F., 2020. Nanoscale Adv. 2, 5106–5129.
Vermeire, S., Van Assche, G., Rutgeerts, P., 2004. Inflamm. Bowel Dis. 10, 661–665.
Wang, S., Song, R., Wang, Z., Jing, Z., Wang, S., Ma, J., 2018. Front. Immunol. 9, 1298.
Wang, X., Mu, Z., Liu, R., Pu, Y., Yin, L., 2013. Food Chem. 141, 3947–3953.
Wu, Z., Hu, X.B., Tao, C.A., Li, Y., Liu, J., Yang, C.D., Shen, D.Z., Li, G.T., 2008. J. Mater. Chem. 18, 5452–5458.